DMSP1.

DMSP, 20151113, F18

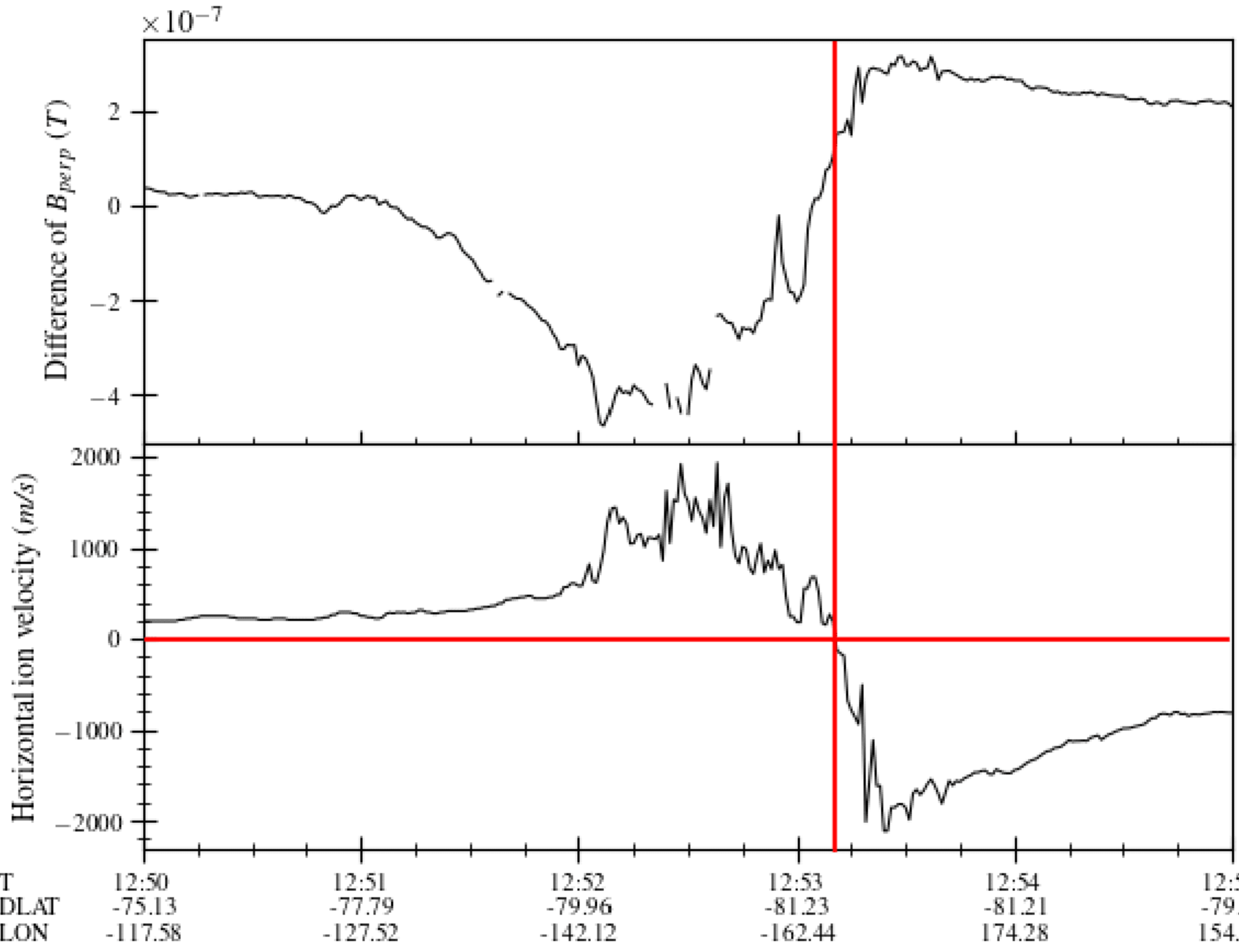

A case study in support of closure of bow shock current through the ionosphere utilizing multi-point observations and simulation

Pauline M. Dredger[1], Ramon E. Lopez[1], Maria Hamrin[2]

[1]University of Texas at Arlington, Arlington, TX, USA
[2]Umeå University, Umeå, Sweden

Key Points:

- Simultaneous, multipoint observations of bow shock current and Birkeland currents are consistent with some closure of the bow shock current through the ionosphere.
- A global MHD simulation of the event is consistent with and supports the conclusions drawn from analysis of the observations.
- We conclude that Birkeland currents flowing on open field lines provide at least partial closure of the bow shock current.

Corresponding author: Pauline M. Dredger, pauline.dredger@mavs.uta.edu

Abstract

On the bow shock in front of Earth flows current due to the curl of interplanetary magnetic field across the shock. It is uncertain whether the bow shock current closes on the magnetopause, into the ionosphere along magnetic field lines, or both. We present simultaneous observations from MMS, AMPERE, and DMSP during a period of strong B_y, weakly negative B_z, and small B_x. This IMF orientation should lead to current flowing mostly south-north on the shock. AMPERE shows current poleward of the Region 1 currents flowing into the northern polar cap and out of the south, consistent with bow shock current closing along open field lines; a DMSP flyover confirms that this current is poleward of the convection reversal boundary. Additionally, we investigate bow shock current closure for these conditions using an MHD simulation. We conclude that the evidence points to partial closure of bow shock current through the ionosphere.

Plain Language Summary

Between Earth and the sun is a region where the solar wind encounters Earth's magnetic field and slows down suddenly, creating a bow shock in space. Across the shock, the magnetic field carried by the solar wind is compressed; this compression means that an electric current flows on the surface of the shock. Although this bow shock current has been observed, there are many uncertainties associated with its closure. This paper discusses simultaneous observations from multiple locations in the magnetosphere of current from the bow shock closing into the polar cap along open magnetic field lines that connect from Earth's magnetic field to the solar wind. The MMS satellite constellation was at the bow shock and observed the direction and magnitude of the bow shock current, while the ACE and THEMIS C spacecraft took measurements of the solar wind upstream of the bow shock. AMPERE calculations, based on data taken in the ionosphere, show current that is the right orientation to be bow shock current flowing into and out of the poles. One of the DMSP satellites observed the same current seen in AMPERE and provides a better description of the current itself and of its location. A simulation of the event based on the available solar wind data confirms the various observations.

1 Introduction

When the supersonic and super-Alfvénic solar wind encounters the earth's magnetic field, it abruptly slows and becomes subsonic, creating the bow shock. Both the solar wind plasma and the interplanetary magnetic field are compressed across the shock. This compression of the magnetic field is associated with a curl of $\vec{B}$ and therefore, by Ampere's law, a current flows on the shock.

Because of the difference in density between the solar wind plasma and the plasma in the magnetosheath, a pressure gradient force points away from the bow shock back into the solar wind. This force does work on the incoming solar wind, converting flow energy into thermal energy. The current due to the compression of the IMF also plays a part in extracting energy from the solar wind flow: it creates a $\vec{J}\times\vec{B}$ force that converts the mechanical energy of the plasma into magnetic energy. The bow shock is always a dynamo or generator, meaning that $\vec{J}\cdot\vec{E} < 0$: although the direction of the bow shock current clearly depends on the orientation of the incoming IMF, the current is always oriented in such a way relative to the IMF that the $\vec{J}\times\vec{B}$ force extracts energy from the solar wind (Lopez et al., 2011).

The bow shock can at times be the primary location in the system where force is exerted against the solar wind. As discussed by Lopez et al. (2010), when the magnetosonic Mach number is high, the pressure gradient force dominates and solar wind energy at the shock is primarily converted to thermal energy; on the other hand, when the Mach number is low, the $\vec{J}\times\vec{B}$ force dominates, so the energy extracted from the flow

is primarily magnetic. In this low Mach number regime, the $\vec{J}\times\vec{B}$ force exerted on the shocked solar wind in the magnetosheath by the interior portion of the Chapman-Ferraro current is balanced by an oppositely directed force from the exterior current. Since under such conditions the magnetopause exerts no net force, via either a pressure gradient or the Chapman-Ferraro current, the force on the solar wind must be mainly provided by the $\vec{J}\times\vec{B}$ force associated with the bow shock current (Lopez & Gonzalez, 2017).

The location of the primary force on the solar wind has consequences for energy transfer throughout the geospace system. Magnetopause reconnection and other load processes require energy to proceed. Lopez et al. (2011) found that for conditions of low Mach number and strongly negative B_z the dynamo that can exist at high latitudes near the cusps disappears; from the discussion in Lopez and Gonzalez (2017), the Chapman-Ferraro current does no work on the magnetosheath plasma at such times. Yet reconnection occurs at the magnetopause for strong southward IMF. During low Mach number conditions, then, the bow shock is the main dynamo in the system and must be the energy source for magnetospheric processes (Siebert & Siscoe, 2002; Lopez & Gonzalez, 2017). This conclusion is supported by the work of Tang et al. (2012), who found that for strong IMF B_z the high latitude magnetopause current decreased while the bow shock current increased.

Poynting flux associated with the bow shock current carries energy away from the shock, so the closure of this current relates to the system of loads and generators in the magnetosphere(Lopez, 2018). Magnetopause reconnection is an obvious place for the bow shock current to close, but various studies have used global MHD simulations to investigate the question and found that the Chapman-Ferraro current is most likely not the only current in the system which can close bow shock current. Lopez et al. (2011) presented evidence that current in the magnetosheath with Region 1 polarity was connected to the bow shock, supporting the argument made by Siscoe et al. (2002) that the Region 1 Birkeland currents are partially closed by the bow shock current. A study by Guo et al. (2008) showed that under strong southward IMF a significant fraction of the Region 1 field-aligned currents could originate from the bow shock. Tang et al. (2009) found that the bow shock current could also contribute to the cross-tail current and power nightside reconnection. In addition to these modeling studies, analysis of MMS (Magnetosphere Multiscale) bow shock crossings by Hamrin et al. (2018) presented observational evidence consistent with closure of the bow shock current across the magnetosheath.

This paper presents a set of observations from various sources consistent with closure of the bow shock current into the ionosphere on open field lines during a single, well-observed event. MMS crossings of the bow shock provide direct measurement of the shock current itself during a time of strong negative B_y and weakly negative B_z. During this period, AMPERE data show unipolar FACS of the right polarity to close the observed bow shock current, while supporting observations from a DMSP flyover in the south pole confirm the existence of Birkeland current poleward of the open-closed boundary. Results from a simulation of the event using the Lyon-Fedder-Mobarry (LFM) global MHD model (Lyon et al., 2004) tell the same story. Taken together, these data and model results give evidence that the bow shock current could be closing through the magnetosheath and also in part through the polar ionosphere.

2 Observations

2.1 Data

The following is a brief description of the datasets used in this study. Solar wind data was compiled from Wind and from THEMIS C (Angelopoulos, 2008). Wind is an upstream solar wind monitor and has orbited at the L1 point since 2004; magnetic field data comes from the Magnetic Field Instrument (MFI) and plasma data from the So-

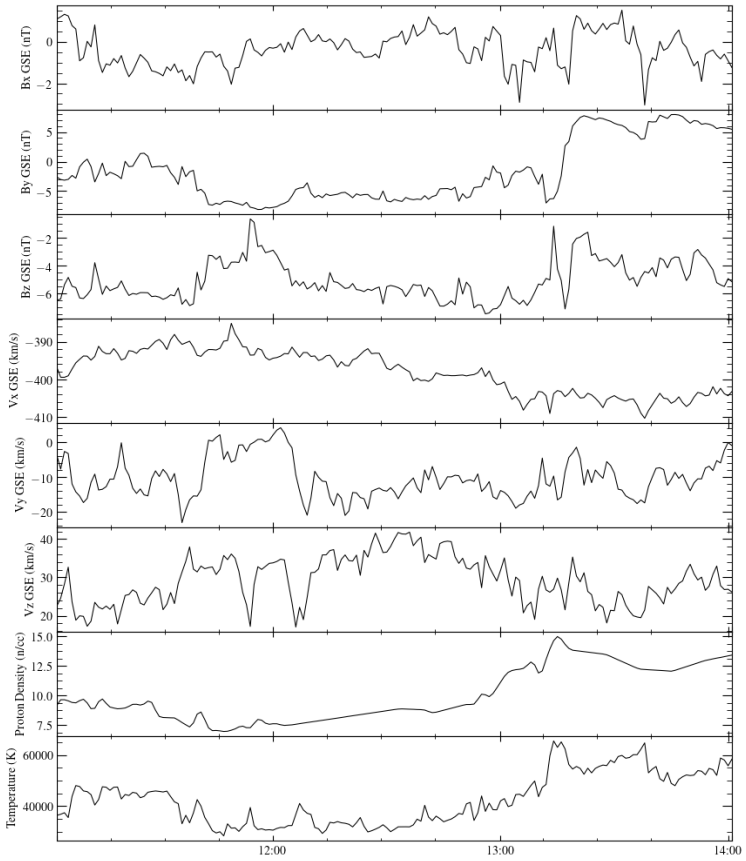

Figure 1. Combined ACE and THEMIS C data, propagated forward 62 minutes to the nominal bow shock. The period of interest is from about 11:45 UT to shortly before 13:00. (Data provided at https://cdaweb.gsfc.nasa.gov/)

lar Wind Experiment (SWE) instrument. THEMIS C is one of the two spacecraft in the ARTEMIS mission and orbits the moon; magnetic field data is taken by the Fluxgate Magnetometer (FGM), while plasma data comes from the Electrostatic Analyzer (ESA) instrument. The MMS (Magnetosphere Multiscale) mission is a constellation of four spacecraft on an elliptical orbit around Earth designed to study magnetic reconnection (Burch et al., 2016). Field-aligned currents are from AMPERE (Active Magnetosphere and Planetary Electrodynamics Response Experiment), a data product from Johns Hopkins University Applied Physics Laboratory that derives ionospheric currents using the magnetic perturbation data from the Iridium communications satellite constellations (Anderson et al., 2014). DMSP (Defense Meteorological Satellite Program) satellites fly on separate polar orbits and provide the Department of Defense with environmental information (Redmann, 1985). Detailed information about the spacecraft and instruments may be found at the websites for the missions listed in the Acknowledgements where the data sources are specified.

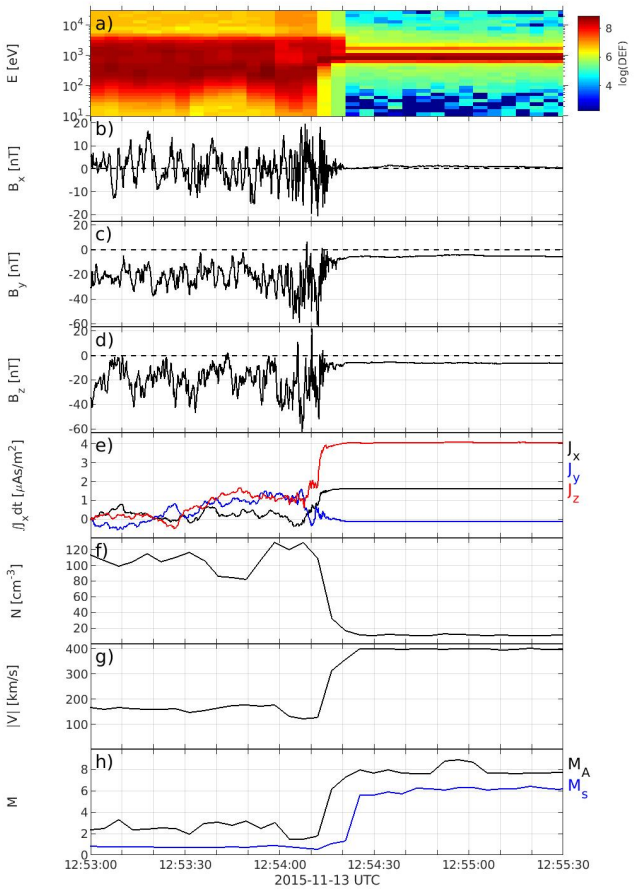

Figure 2. MMS observations of the bow shock. The spacecraft encountered the shock between 12:54:10 and 12:54:20 UT.

2.2 Solar Wind Conditions During the Event

The coordinates used in this paper for all the spacecraft with the exception of DMSP-F18 are Geocentric Solar Ecliptic (GSE) coordinates, where the X-axis points from Earth to the sun, the Y-axis is in the ecliptic plane, and the Z-axis is perpendicular to both, pointing northward. Between 11:45 and 13:15 UT on November 13, 2015, IMF B_x was close to zero, while B_z was weakly negative. B_y was between -5 nT and -8 nT but was overall pretty steady during this period. Solar wind velocities were steady, as were the temperature and pressure. The fact that B_y dominated the IMF during the event means that the bow shock current should have been flowing mostly south to north, as determined by the curl of $\vec{B}$ across the shock.

Wind was supplying the OMNI data in the period of interest, but there were a couple of significant gaps at important times. For this reason, we considered the event with reference to ACE observations, which were more complete except for a total lack of proton density measurements. The two satellites were around 80 R_E apart in X, less than 40 R_E apart in Y, and roughly 8 R_E apart in Z. THEMIS C was close to the Earth-sun line during this period. Based on a comparison between ACE and THEMIS magnetic

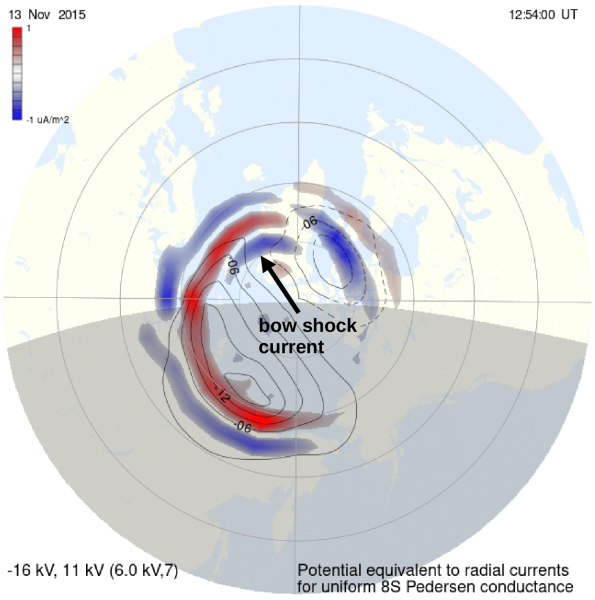

Figure 3. AMPERE derived Birkeland currents for the northern hemisphere. Red currents are upward, blue currents are downward. We see high latitude unipolar current (indicated) in the afternoon sector in the north with the right polarity to be bow shock current closing into the ionosphere. The northern hemisphere plot has the MIX ionospheric potential contours plotted. (Plot from http://ampere.jhuapl.edu/)

field data, THEMIS C seemed to be seeing the same solar wind that ACE saw but approximately 48 minutes later. We were therefore able to replace the missing ACE densities (between 0950 UT and 1300 UT) with those observed by THEMIS C (time-shifted by 48 minutes), after which we propagated the combined dataset forward 62 minutes, to line up with available OMNI data. The resulting combined solar wind data time series is shown in Figure 1 and this solar wind time series, which was used to drive the LFM simulation, can be replicated using the information provided here and the archived ACE and THEMIS C data.

2.3 MMS Observations of the Bow Shock

Figure 2 shows MMS data from 12:53:00 to 12:55:30 UT, near the end of the period described above. Shortly before 12:51 UT (not shown), the MMS constellation crossed the bow shock into the magnetosheath, where it remained for roughly three and a half minutes before crossing back into the solar wind right after 12:54 UT, as shown. This encounter with the shock occurred at (X,Y,Z) = (9.7, 5.2, -0.9) R_E, relatively close to the nose. The compression of the magnetic field (panels b, c, d), the decrease in the ion density (panel f), and the increase in the ion velocity (panel g) across the shock are consistent with the data from ACE at the observed magnetosonic Mach number (panel h). This agreement means that the solar wind data we infer from ACE and THEMIS C are indeed the real conditions directly upstream of the bow shock, a fact that becomes crucial when we simulate the event with an MHD model using these data as input. Panel e of Figure 2 shows the current density components integrated along the spacecraft path; the dominant component is J_z with some contribution from J_y. Thus, MMS observed a tilted south to north current as the spacecraft crossed the bow shock.

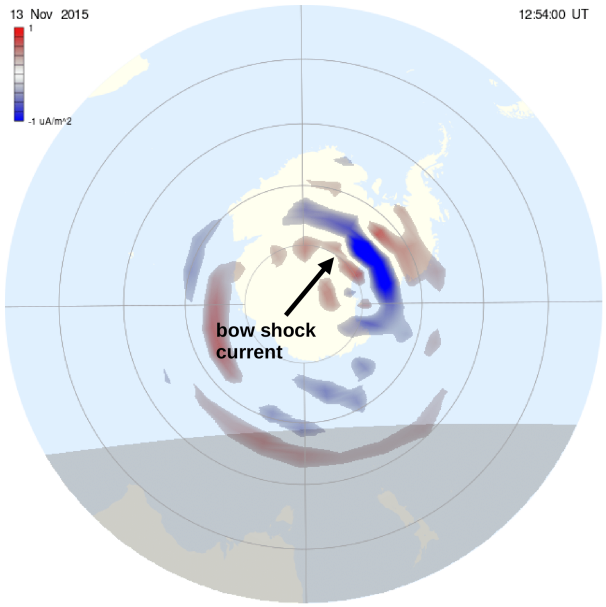

Figure 4. AMPERE derived Birkeland currents for the southern hemisphere. Red currents are upward, blue currents are downward. We see high latitude unipolar current (indicated) in the morning sector in the south with the right polarity to be bow shock current closing into the ionosphere. (Plot from http://ampere.jhuapl.edu/)

2.4 AMPERE and DMSP Observations of Field-Aligned Currents

The AMPERE-derived Birkeland (field-aligned) currents are shown in Figure 3 and 4; red indicates current coming out of the ionosphere (upward) and blue current is flowing into the ionosphere (downward). The projection is known as "glass-Earth", so that the view in both cases is from the perspective of an observer above the north pole. The southern polar cap view is as if the observer were looking through a transparent Earth. In each view noon is at the top of the figure, dawn to the right, and dusk to the left. We can see the Region 1 current flowing into the ionosphere (blue) in the dawn sector and out (red) in the dusk sector, while at lower latitudes are the Region 2 currents, of opposite polarity to Region 1. At the time of MMS's encounter with the bow shock, AMPERE data show a unipolar current region poleward of the Region 1 Birkeland current patterns in both northern and southern hemispheres. This current flows into the northern polar cap and out of the south at high latitudes. Figure 3 shows the AMPERE observations for the north pole at 12:54, when MMS crossed the bow shock back into the solar wind, and the southern observations are shown in Figure 4. We can see in the northern afternoon sector a substantial downward current separate from the Region 1 current and in the southern morning sector an upward current at correspondingly high latitudes. These FACs are of the right polarity – downward (blue) in the north and upward (red) in the south – to close the south-north bow shock current observed by MMS, if those currents are on open field lines. The critical point, then, is to find the position of these Birkeland currents relative to the open-closed field line boundary.

For this event, we can determine the location of the open-closed boundary at least in one hemisphere by means of ion driftmeter data from DMSP. During the period in which MMS crossed the bow shock, F18 was making an overpass of the southern polar cap and flew right through the high latitude upward current seen by AMPERE and discussed above, as shown in Figure 4. The top panel of Figure 5 shows the difference be-

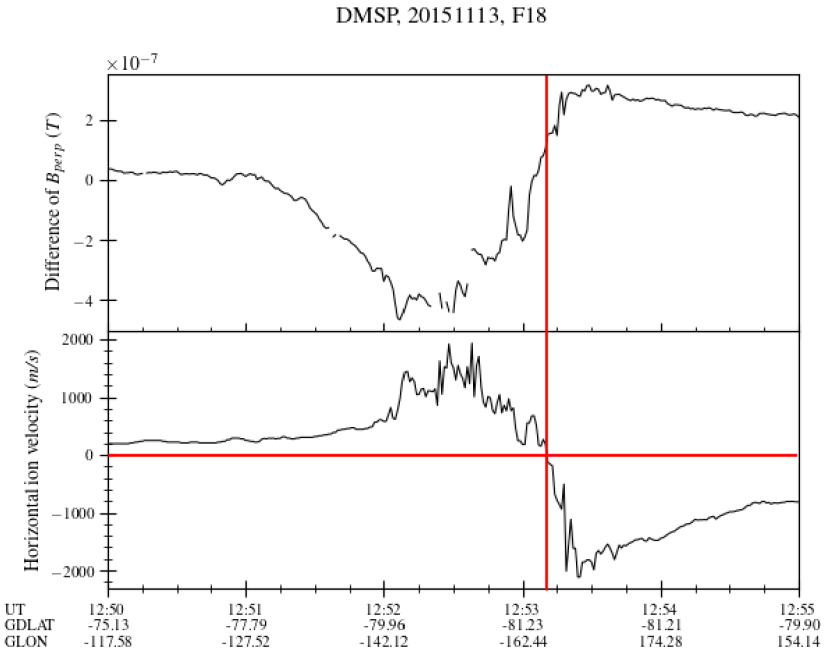

Figure 5. F18 observations: difference of B_{perp} and horizontal ion drift velocities. After the ion velocities turn negative shortly after 12:54 UT, marking the convection reversal boundary, we see some magnetic field perturbations, indicative of current flowing on open field lines. (Data provided at http://cedar.openmadrigal.org/list/)

tween the observed magnetic field and the IGRF model perpendicular to the flight track of F18, which gives an estimate of the magnetic perturbation resulting from Birkeland currents. The bottom panel is a plot of the horizontal ion drift velocities, from which we can determine the convection reversal boundary by noting where the plasma velocities turn negative. Negative velocities correspond to open field lines being dragged toward the nightside and the plasma flowing with them, whereas positive velocities are associated with closed field lines and plasma moving toward the dayside. By this reasoning, we can say that F18 encountered the open-closed boundary a few seconds after 12:53. From the magnetic field perturbations observed after the satellite passes through the boundary, we infer that part of the upward current through which F18 flew was flowing on open field lines. The particle precipitation data in Figure 6 shows a clear auroral oval with an open polar cap, consistent with southward IMF. Just after 12:52 we see an intense downward flux of low energy electrons that corresponds to an upward Birkeland current. We also see some precipitating ions, but after F18 crosses the open-closed boundary at 12:53 the ions disappear. Only a distinct electron population remains; its spectrum, shown in Figure 7, is a low-energy accelerated Maxwellian. This is the signature of electrons carrying an upward current with a field-aligned potential accelerating the electrons downward to the velocity required to carry the current, which in this case was on open field lines. In short, the DMSP observations confirm that in the southern hemisphere there

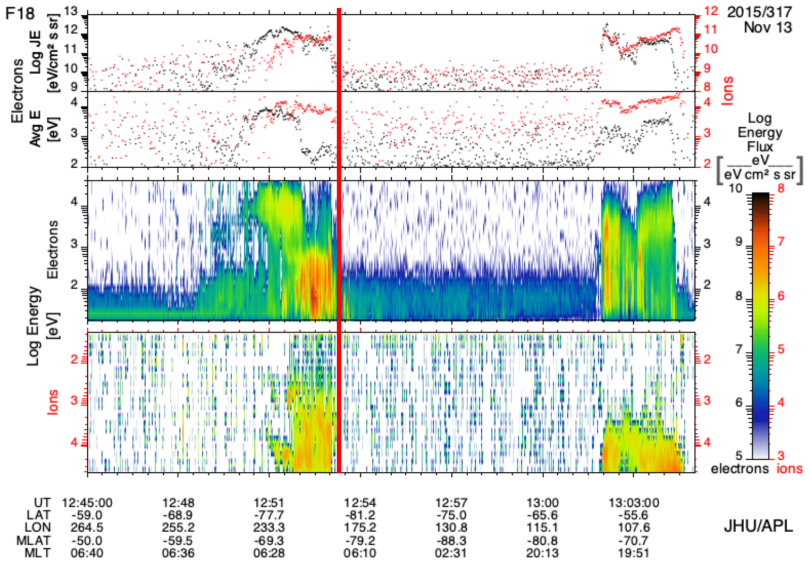

Figure 6. F18 particle precipitation data over the southern polar cap. The red line indicates when the spacecraft crossed the convection reversal boundary at 12:53 UT. (Plot from http://sd-www.jhuapl.edu/Aurora/spectrogram/)

Figure 7. Spectrum of the particle precipitation seen at 12:53:37 in Figure 6. The accelerated Maxwellian seen in the electron spectrum indicates electrons being pushed upward in a current. (Plot from http://sd-www.jhuapl.edu/Aurora/spectrogram/)

was current at the location seen by AMPERE and of the same orientation, poleward of the convection reversal boundary and therefore on open field lines.

3 Results from the MHD Simulation

The MHD model used in this study was the Lyon-Fedder-Mobarry (LFM) global MHD model (Lyon et al., 2004), and the version of LFM used in this study was LFM-MIX (Magnetosphere-Ionosphere Coupler Solver) (Merkin & Lyon, 2010). LFM solves the ideal MHD equations on a logically orthogonal, distorted spherical meshed grid. There is a higher density of grid points in areas of special interest, such as where the magnetopause and bow shock are typically located. The grid point separation in these areas is about 0.25 R_E. In the areas of the distant magnetotail and upstream of the bow shock, where the solar wind enters the grid space, the grid separation is about 1.25 R_E. The grid space extends from $-30R_E < X < 350R_E$ (in GSE) and is cylindrically wrapped to $Y, Z < 130R_E$. At the inner boundary, the field-aligned currents are calculated at that altitude from the curl of B and mapped to ionospheric altitudes where the height-integrated electrostatic equation is solved for the ionospheric potential. The ionospheric electric field is then mapped back to the MHD grid to provide a boundary condition for Faraday's Law and for the perpendicular velocity. As mentioned above, we are confident, because of the MMS observations right outside the bow shock, that the solar wind conditions seen by ACE/THEMIS C, propagated forward to a nominal shock position, accurately represent the real conditions at the bow shock during the event and thus are

the correct input to the simulation for the event. We used the propagated ACE/THEMIS C dataset described in Section 2.2 to drive LFM-MIX at quad resolution.

The model correctly predicts the location of the bow shock at the time of the crossing by MMS. Figure 8 shows the modeled conditions at the MMS crossing position for the twenty minutes around the time of the event. Although the simulation output is of a much lower resolution than the actual data, we can see that the simulated bow shock does indeed pass over the satellite shortly before 13:00 UT; both magnetic field and plasma parameters change rapidly from magnetosheath values to values corresponding to the solar wind input conditions at the time. The modeled crossing is actually a few minutes after the real crossing. Additionally, before the 12:54 UT crossing MMS encountered the bow shock a handful of times in quick succession. These minor discrepancies can be due to uncertainties in solar wind timing and the spatial resolution of LFM versus the actual thickness of the bow shock. Broadly speaking, however, the bow shock was in the right position at the right time in the simulation output.

The simulated field-aligned currents from MIX are shown in Figure 9. In the northern hemisphere plot, red currents are downward and blue currents are upward (opposite to the AMPERE plots), while in the southern hemisphere red currents are upward and blue currents are downward (matching AMPERE). Unlike the AMPERE images, in which dawn is on the right in both hemispheres, the southern MIX plot is not mirrored, so dawn is on the left in the south. The simulated FACs are generally similar to observations; in particular, the model reproduces the high latitude knots of current seen by AMPERE that seem to be flowing along open field lines. The modeled currents are similar in magnitude, though a bit larger than the AMPERE-derived currents, but it is known that MIX tends to overestimate the cross polar cap potential, which would explain this discrepancy (Wiltberger et al., 2012).

To determine whether or not the modeled high latitude current in the southern hemisphere is poleward of the open-closed boundary, as was the current for which we have DMSP observations, we traced a magnetic field line from the current knot of interest. To do the tracing, we mapped the field line from the MIX ionosphere to the inner boundary of LFM and then used this location as the seed point for a stream tracer. The stream tracer generates field lines by tracing curves that are instantaneously tangential to a vector field, which in this case was the magnetic field $\vec{B}$. One such field line (half colored white) is visible in Figure 11 and is undoubtedly open. The high latitude southern hemisphere red current is flowing at least partially on open field lines, both in observations and in the model. Moreover, the AMPERE plot for the northern hemisphere includes the potential contours from the MIX model (not available for the southern hemisphere) and it can be seen that the northern counterpart of the southern hemisphere current discussed above was in a region of antisunward plasma flow, poleward of the convection reversal boundary. Therefore, the global simulation of the event and the observations are in agreement that the high latitude Birkeland current with polarity consistent with bow shock current closure was flowing on open field lines.

4 Discussion and Conclusions

In this paper, we have presented a set of coordinated observations of the bow shock and low altitude Birkeland currents on November 13, 2015, during a period when the IMF was dominated by the B_y component. The MMS data show the primarily south-to-north current at the bow shock, while DMSP and Ampere show upward Birkeland current in the southern hemisphere at high latitudes in the MMS local time sector. Moreover, the DMSP data show that some of the Birkeland current was flowing in the polar cap on open field lines, and as such would connect to currents in the magnetosheath. These observations are consistent with the hypothesis that, in this case, some of the bow shock current was closing across the magnetosheath into the ionosphere.

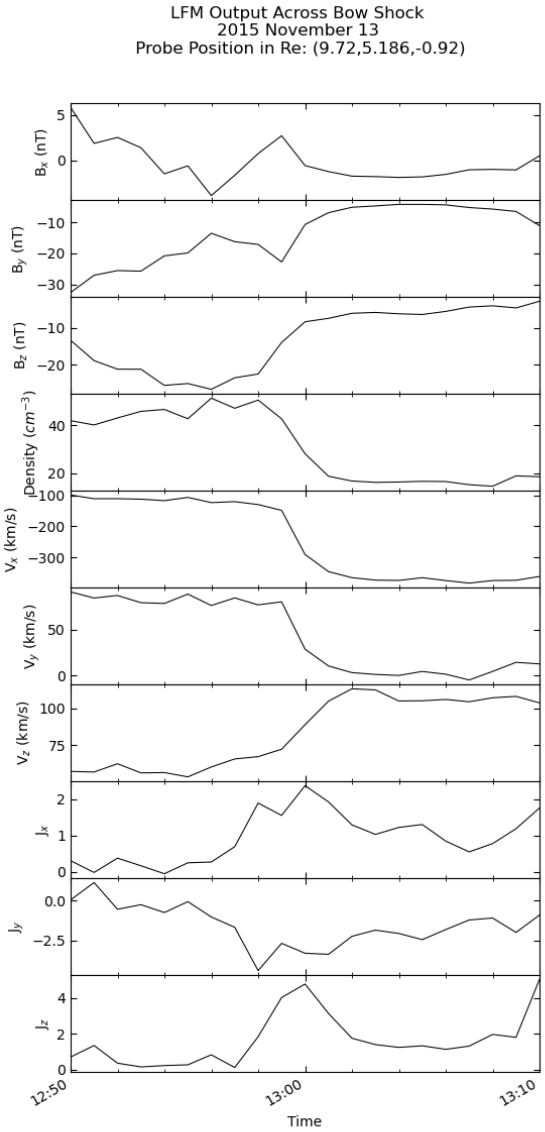

Figure 8. LFM output at the MMS crossing location for the 20 minutes around the crossing time on 2015/11/13. The bow shock crossed the probe position, which was that of MMS at the time of the 12:54 UT crossing, between 12:58 and 13:02 UT. Current density components are in arbitrary units.

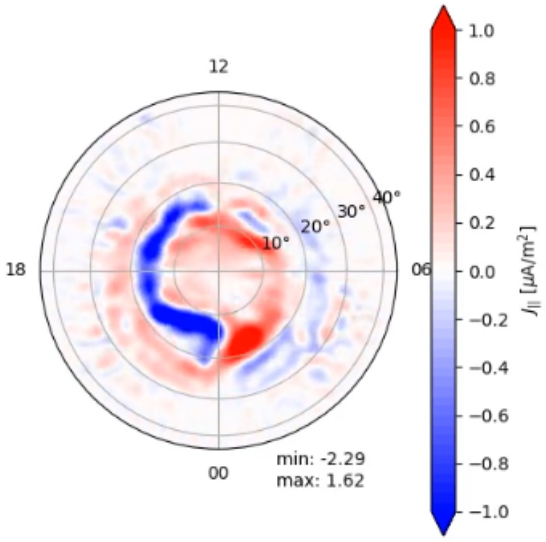

Figure 9. Northern hemisphere modeled FACs. Red current is flowing into the ionosphere, blue is flowing out.

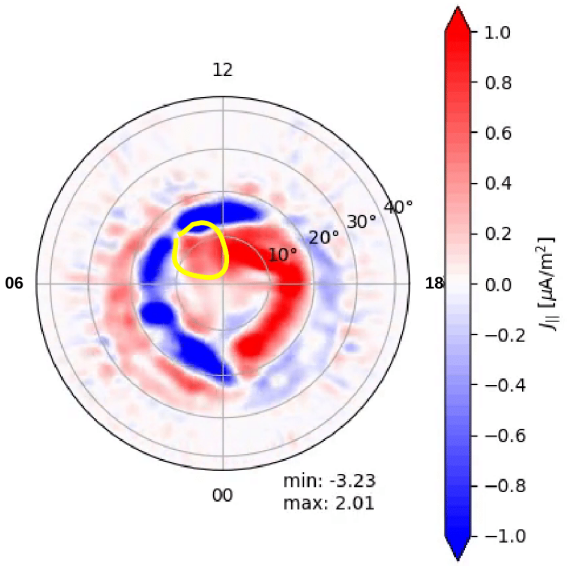

Figure 10. Southern hemisphere modeled FACs, where the circled current indicates the point of the field line tracing. Here, blue current is flowing into the ionosphere (opposite convention to the northern plot).

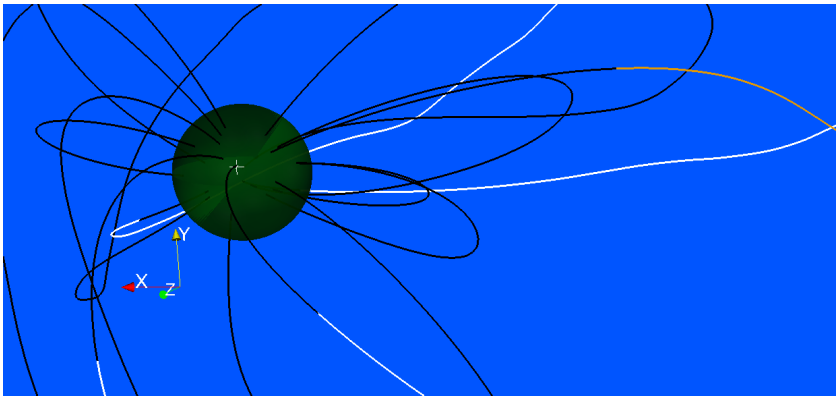

Figure 11. Field line tracing from the Birkeland current circled in Figure 9b. The white colored streamlines indicate open magnetic field lines.

The event has been simulated with the LFM global magnetosphere model. The simulation puts the bow shock in the right place at essentially the right time. The Birkeland current pattern in the simulation is generally similar to the pattern derived by AMPERE, particularly with respect to the high latitude Birkeland current that is of the correct polarity to close part of the bow shock current. Moreover, field line tracing indicates that some of this Birkeland current is on open field lines that go into the magnetosheath. Given observations of the predicted bow shock current, a Birkeland current of the correct polarity to close the bow shock current that is at least partially on open field lines, and support from a global MHD simulation showing the same results, we believe that the evidence is strongly in favor of the closure through the polar cap ionosphere of at least part of the bow shock current.

Many questions remain about bow shock current closure. If the bow shock current is closing in part through the ionosphere with the Birkeland currents, where does it cross the magnetosheath? Does it flow back towards the nightside first, or does it begin to flow along open field lines on or close to the dayside? We should also investigate the relationship of the bow shock current with the Chapman-Ferraro current and what role the magnetopause plays or does not play in bow shock current closure. It is probable that the nature of this closure depends largely on prevailing conditions. The IMF clock angle dictates the direction of the bow shock current and thus clearly regulates its closure. The magnetosonic Mach number may be particularly important, since it affects the location of the primary force exerted on the solar wind and the main dynamo in the system. In addition, ionospheric conductance must influence the ability of the bow shock current to close into the polar cap. Further study is needed to examine the interconnected system of currents, conductance, and solar wind conditions.

Acknowledgments

We acknowledge the support of the US National Science Foundation (NSF) under grant 1916604. We also acknowledge the support of the National Aeronautics and Space Administration (NASA) under grants 80NSSC19K1670 and 80NSSC20K0606 (The Center for the Unified Study of Interhemispheric Asymmetries (CUSIA)). M. Hamrin was supported by the Swedish National Space Agency and the Swedish Research Council.

ACE and THEMIS data (https://cdaweb.sci.gsfc.nasa.gov/index.html/) were provided by V. Angelopoulos, C.W. Carlson, & J. McFadden at UCB; U. Auster & K.H.

Glassmeier at TUBS; and W. Baumjohann at IWF, supported through NASA contract NAS5-02099 and the BMWi and DLR contract 50 OC 0302.

We thank the AMPERE team and the AMPERE Science Center for providing the Iridium derived data products (http://ampere.jhuapl.edu/).

The DMSP SSJ/4 particle detectors were designed by Dave Hardy of AFRL. Those data and the plots that show the data were obtained from JHU/APL at http://sd-www.jhuapl.edu/Aurora/spectr The DMSP plasma drift and magnetometer data were obtained from http://cedar.openmadrigal.org and we thank Dr. Patricia Doherty for conversations concerning those data.

We thank the MMS Science Data Center and the MMS teams, especially the magnetic field and the ion teams, for producing high quality data. We also acknowledge NASA's National Space Science Data Center and Space Physics Data Facility. MMS data are available at https://lasp.colorado.edu/mms/sdc/public/.

References

Anderson, B. J., Korth, H., Waters, C. L., Green, D. L., Merkin, V. G., Barnes, R. J., & Dyrud, L. P. (2014). Development of large-scale birkeland currents determined from the active magnetosphere and planetary electrodynamics response experiment. *Geophysical Research Letters*, *41*(9), 3017-3025. doi: https://doi.org/10.1002/2014GL059941

Angelopoulos, V. (2008). The themis mission. *Space Science Reviews*, *141*(1), 5. doi: 10.1007/s11214-008-9336-1

Burch, J. L., Moore, T. E., Torbert, R. B., & Giles, B. L. (2016). Magnetospheric multiscale overview and science objectives. *Space Science Reviews*, *199*(1), 5–21. doi: 10.1007/s11214-015-0164-9

Guo, X. C., Wang, C., Hu, Y. Q., & Kan, J. R. (2008). Bow shock contributions to region 1 field-aligned current: A new result from global mhd simulations. *Geophysical Research Letters*, *35*(3). doi: 10.1029/2007GL032713

Hamrin, M., Gunell, H., Lindkvist, J., Lindqvist, P.-A., Ergun, R. E., & Giles, B. L. (2018). Bow shock generator current systems: Mms observations of possible current closure. *Journal of Geophysical Research: Space Physics*, *123*(1), 242-258. doi: 10.1002/2017JA024826

Lopez, R. E. (2018). The bow shock current system. In *Electric currents in geospace and beyond* (p. 477-496). American Geophysical Union (AGU). doi: https://doi.org/10.1002/9781119324522.ch28

Lopez, R. E., Bruntz, R., Mitchell, E. J., Wiltberger, M., Lyon, J. G., & Merkin, V. G. (2010). Role of magnetosheath force balance in regulating the dayside reconnection potential. *Journal of Geophysical Research: Space Physics*, *115*(A12). doi: 10.1029/2009JA014597

Lopez, R. E., & Gonzalez, W. D. (2017, April). Magnetospheric balance of solar wind dynamic pressure. *Geophysical Research Letters*, *44*(7), 2991-2999. doi: 10.1002/2017GL072817

Lopez, R. E., Merkin, V. G., & Lyon, J. G. (2011, June). The role of the bow shock in solar wind-magnetosphere coupling. *Annales Geophysicae*, *29*(6), 1129-1135. doi: 10.5194/angeo-29-1129-2011

Lyon, J., Fedder, J., & Mobarry, C. (2004, 10). The lyon-fedder-mobarry (lfm) global mhd magnetosphere simulation code. *Journal of Atmospheric and Solar-Terrestrial Physics*, *66*, 1333-1350. doi: 10.1016/j.jastp.2004.03.020

Merkin, V. G., & Lyon, J. G. (2010). Effects of the low-latitude ionospheric boundary condition on the global magnetosphere. *Journal of Geophysical Research: Space Physics*, *115*(A10). doi: https://doi.org/10.1029/2010JA015461

Redmann, J. (1985). An overview of the mission sensor systems of the dmsp satellites. In *23rd aerospace sciences meeting* (p. 240).

366 Siebert, K. D., & Siscoe, G. L. (2002). Dynamo circuits for magnetopause reconnec-
367 tion. *Journal of Geophysical Research: Space Physics*, *107*(A7), SMP 6-1-SMP
368 6-5. doi: 10.1029/2001JA000237
369 Siscoe, G. L., Crooker, N. U., & Siebert, K. D. (2002). Transpolar potential satura-
370 tion: Roles of region 1 current system and solar wind ram pressure. *Journal of*
371 *Geophysical Research: Space Physics*, *107*(A10), SMP 21-1-SMP 21-8. doi: 10
372 .1029/2001JA009176
373 Tang, B. B., Guo, X. C., Wang, C., Hu, Y. Q., & Kan, J. R. (2009). Bow shock
374 and magnetopause contributions to the cross-tail current from global mhd
375 simulations. *Journal of Geophysical Research: Space Physics*, *114*(A8). doi:
376 10.1029/2009JA014325
377 Tang, B. B., Wang, C., & Guo, X. C. (2012). Bow shock and magnetopause con-
378 tributions to the magnetospheric current system: Hints from the cluster ob-
379 servations. *Journal of Geophysical Research: Space Physics*, *117*(A1). doi:
380 https://doi.org/10.1029/2011JA016681
381 Wiltberger, M., Qian, L., Huang, C.-L., Wang, W., Lopez, R. E., Burns, A. G., ...
382 Huang, Y. (2012). Cmit study of cr2060 and 2068 comparing l1 and mas
383 solar wind drivers. *Journal of Atmospheric and Solar-Terrestrial Physics*,
384 *83*, 39-50. (Corotating Interaction Regions from Sun to Earth: Modeling
385 their formation, evolution and geoeffectiveness) doi: https://doi.org/10.1016/
386 j.jastp.2012.01.005

LFM Bow Shock.

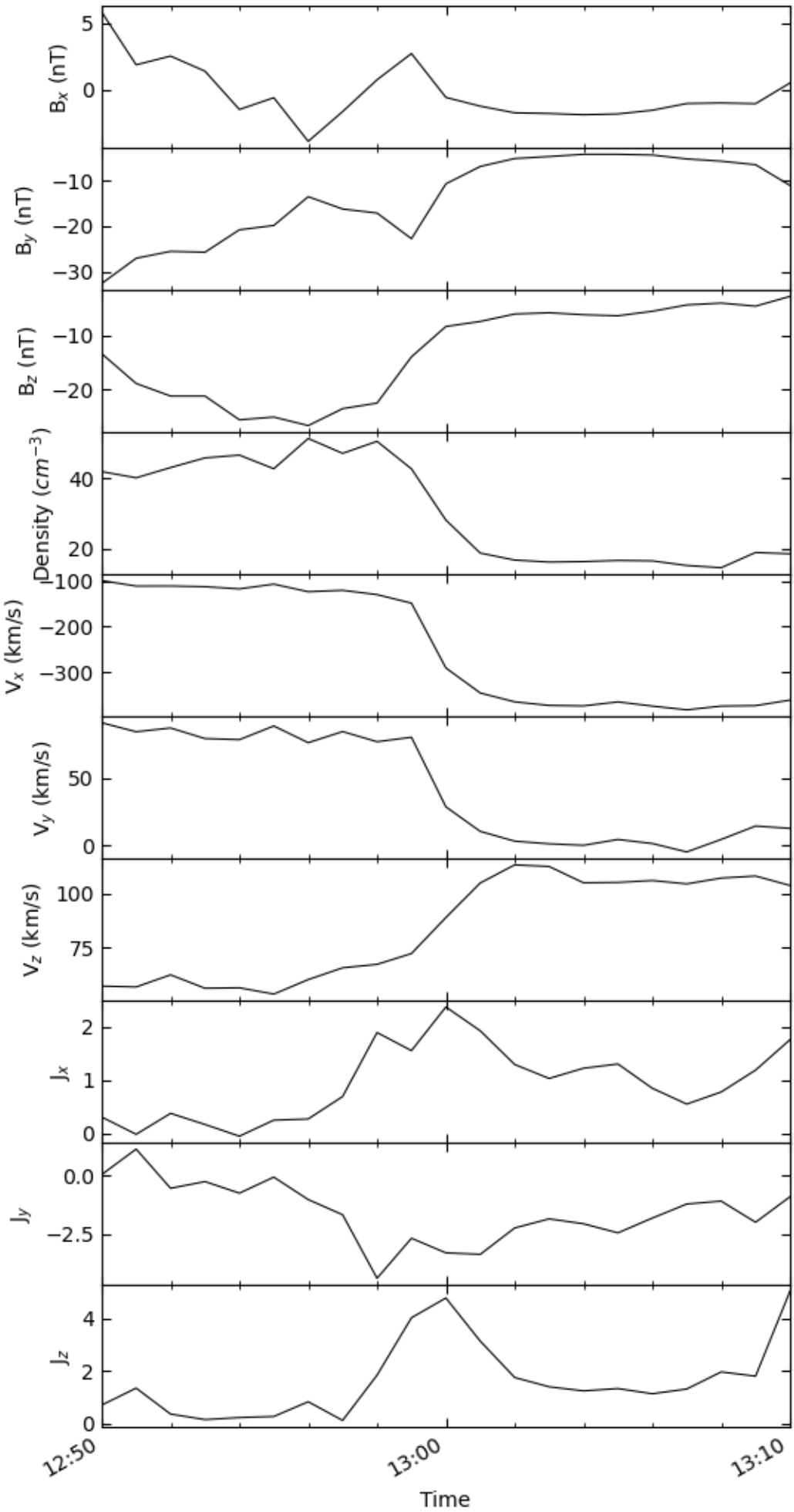
LFM Output Across Bow Shock
2015 November 13
Probe Position in Re: (9.72,5.186,-0.92)
B_x (nT)
B_y (nT)
B_z (nT)
Density (cm^{-3})
V_x (km/s)
V_y (km/s)
V_z (km/s)
J_x
J_y
J_z
12:50
13:00
13:10
Time

MIX North.

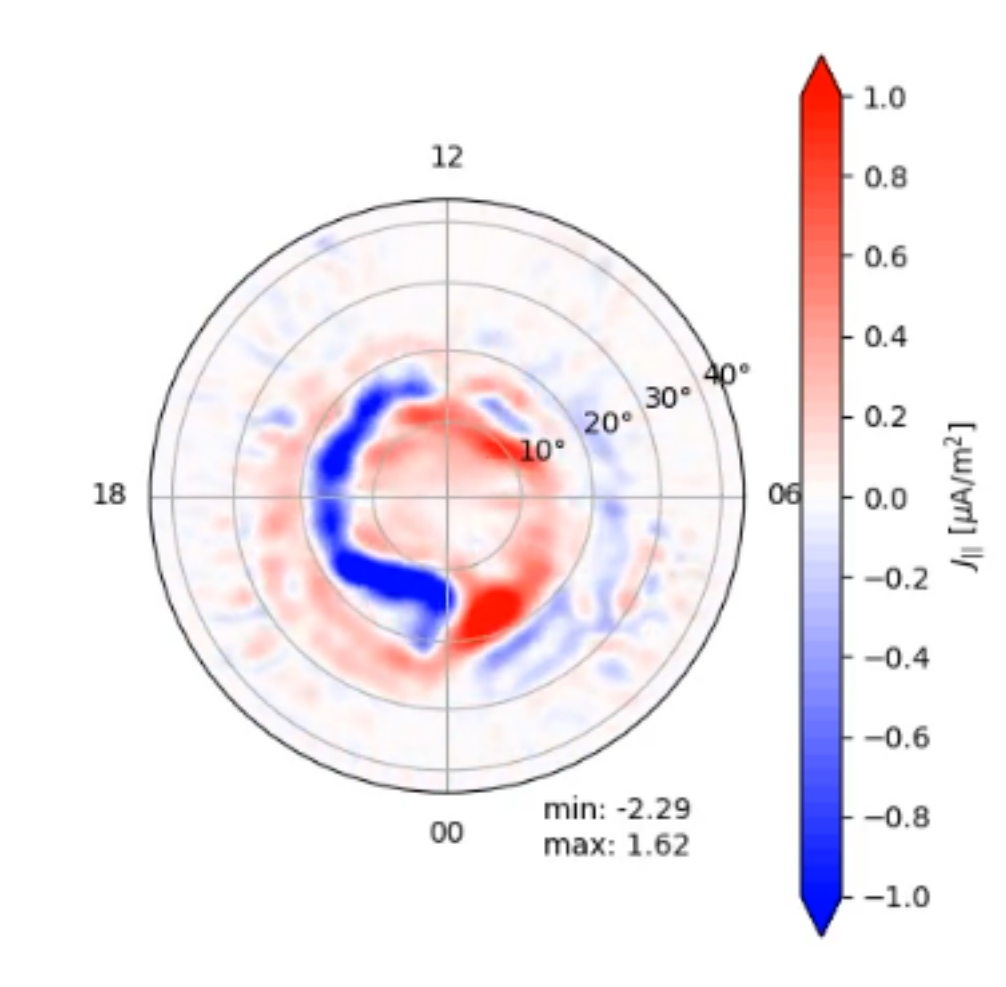
12
18
06
00
10°
20°
30°
40°
min: -2.29
max: 1.62
1.0
0.8
0.6
0.4
0.2
0.0
−0.2
−0.4
−0.6
−0.8
−1.0
$J_{\parallel}$ [μA/m^2]

MMS.

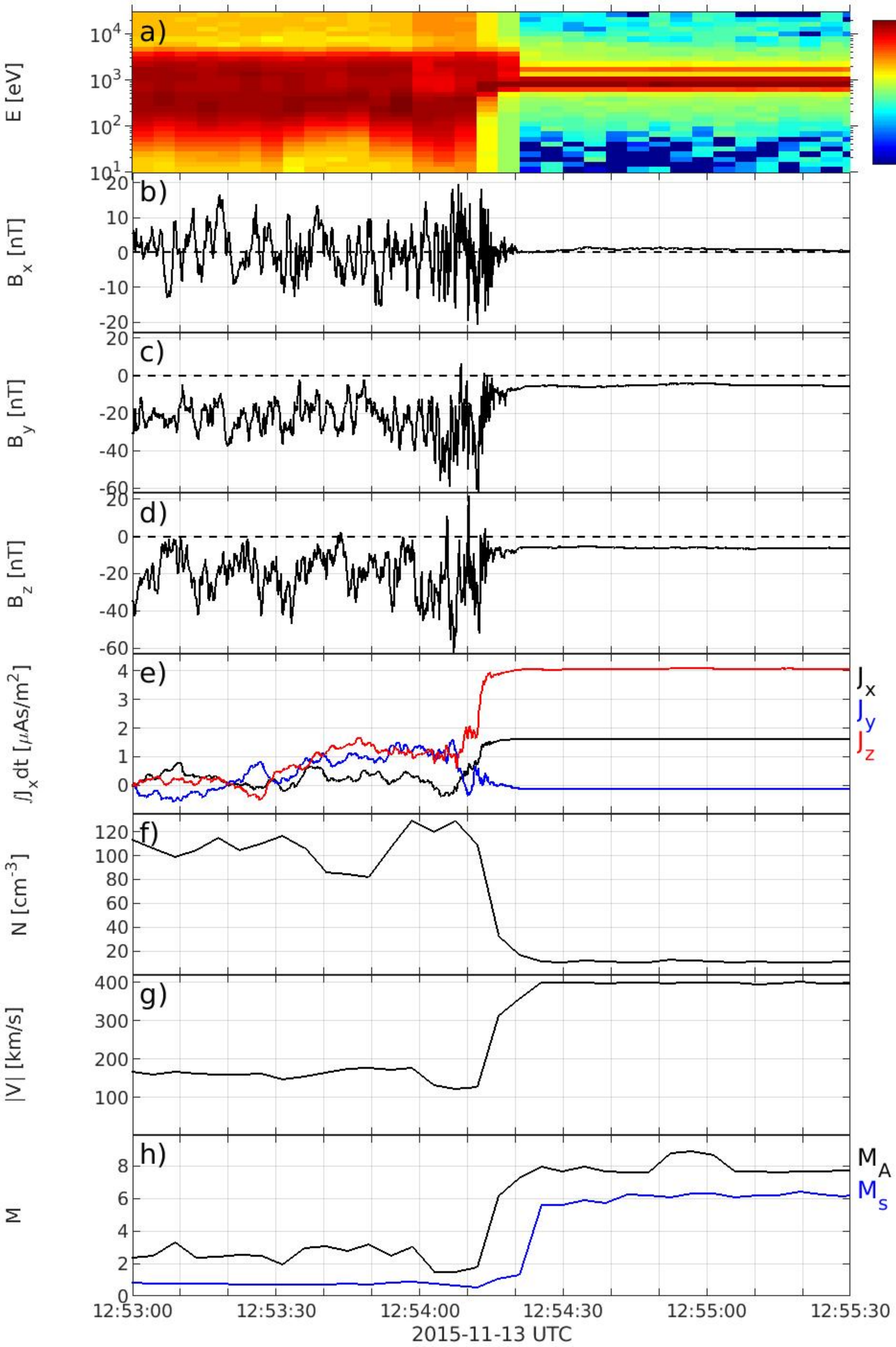
a)
E [eV]
10^4
10^3
10^2
10^1
log(DEF)
8
6
4
b)
B_x [nT]
20
10
0
-10
-20
c)
B_y [nT]
20
0
-20
-40
-60
d)
B_z [nT]
20
0
-20
-40
-60
e)
$\int J_x dt$ [μAs/m^2]
4
3
2
1
0
J_x
J_y
J_z
f)
N [cm^{-3}]
120
100
80
60
40
20
g)
|V| [km/s]
400
300
200
100
h)
M
8
6
4
2
0
M_A
M_s
12:53:00
12:53:30
12:54:00
12:54:30
12:55:00
12:55:30
2015-11-13 UTC

AMPERE North.

13 Nov 2015

12:54:00 UT

1

-1 uA/m^2

06

-06

bow shock
current

-12

06

-16 kV, 11 kV (6.0 kV,7)

Potential equivalent to radial currents
for uniform 8S Pedersen conductance

AMPERE South.

13 Nov 2015

12:54:00 UT

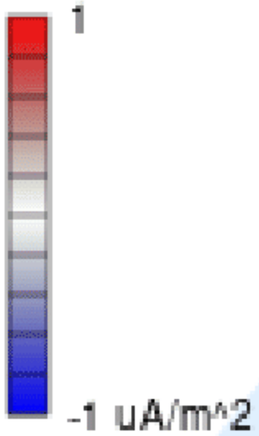

bow shock
current

Solar Wind.

Propagated Solar Wind from ACE

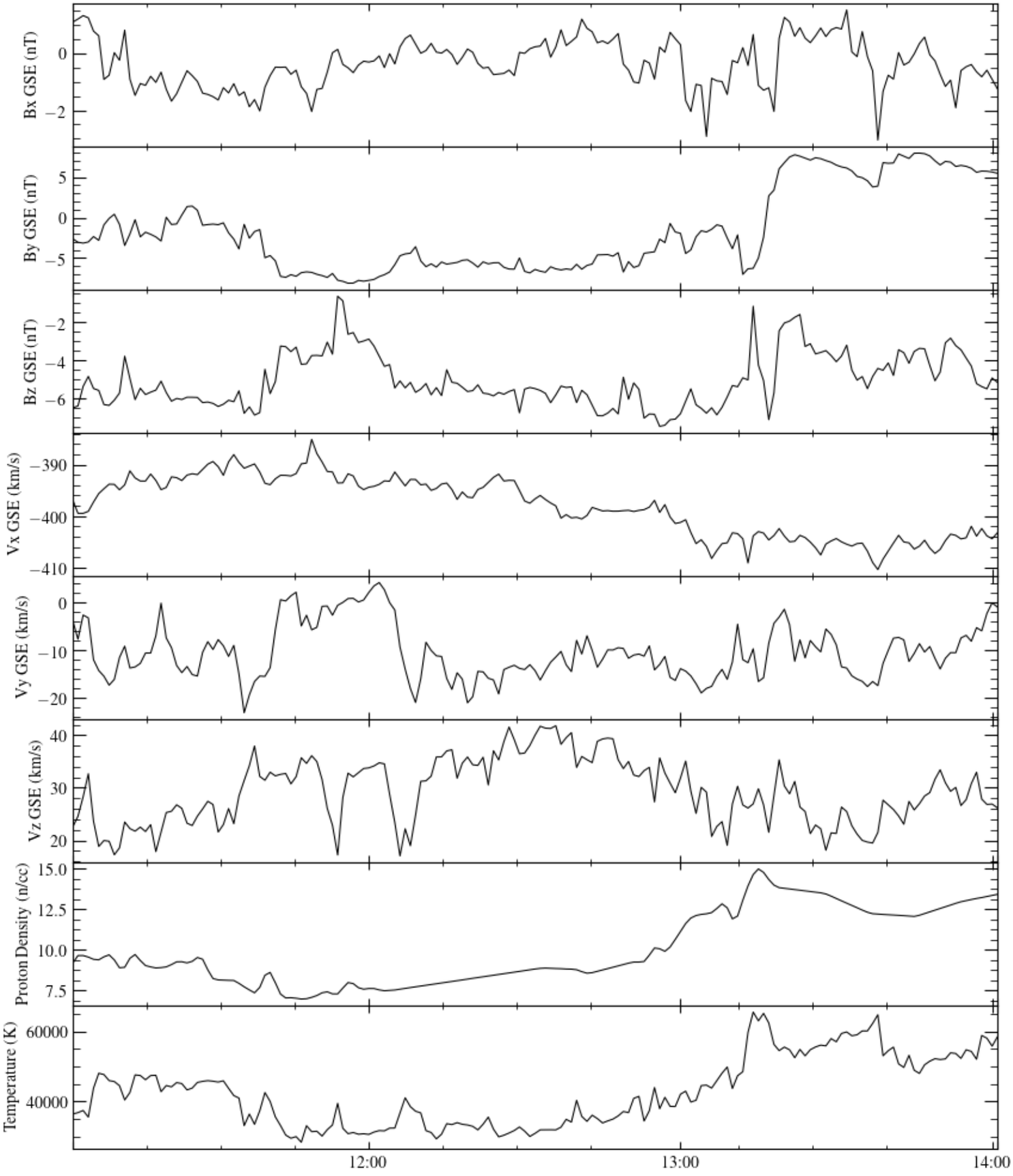

LFM Field Line.

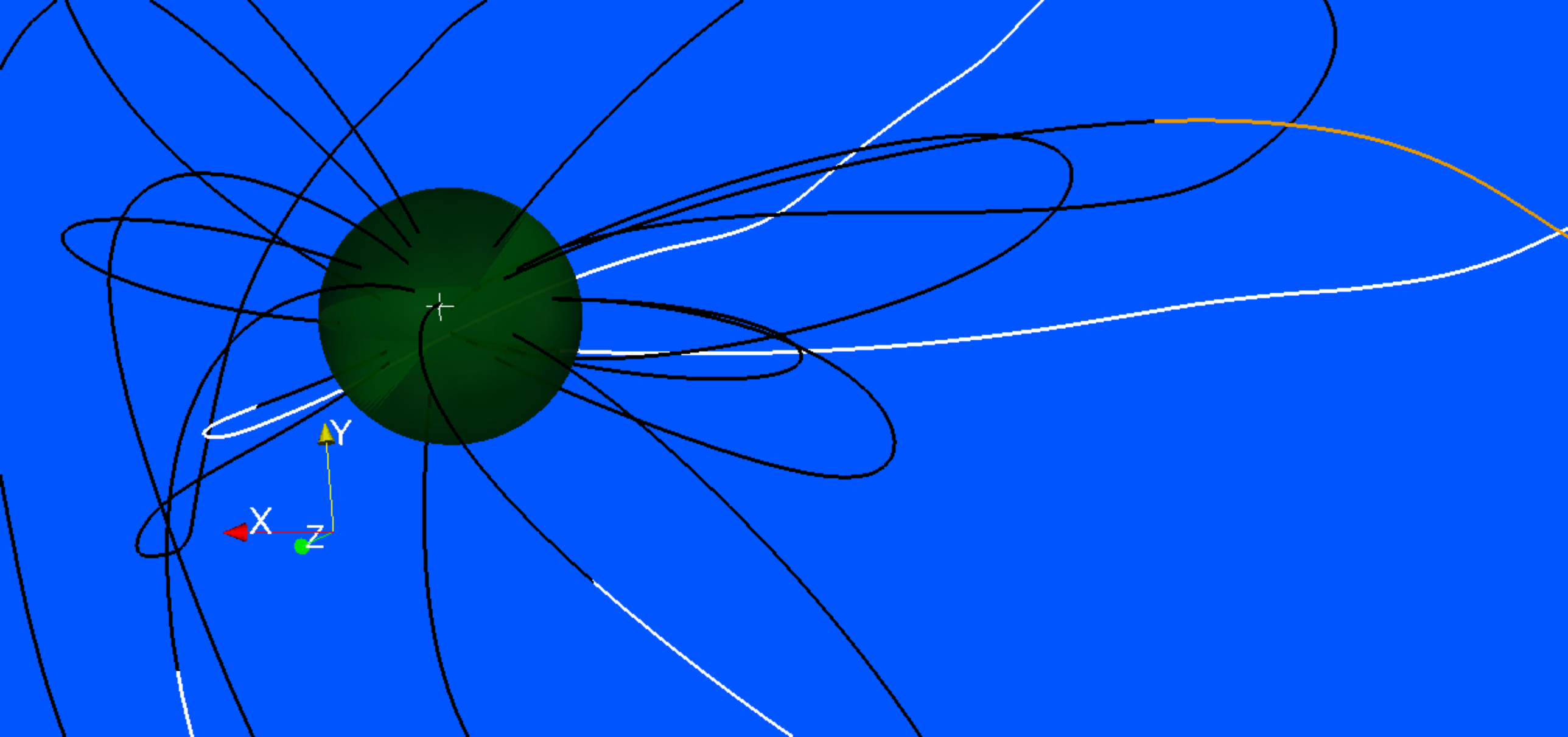
Y
X
Z

DMSP2.

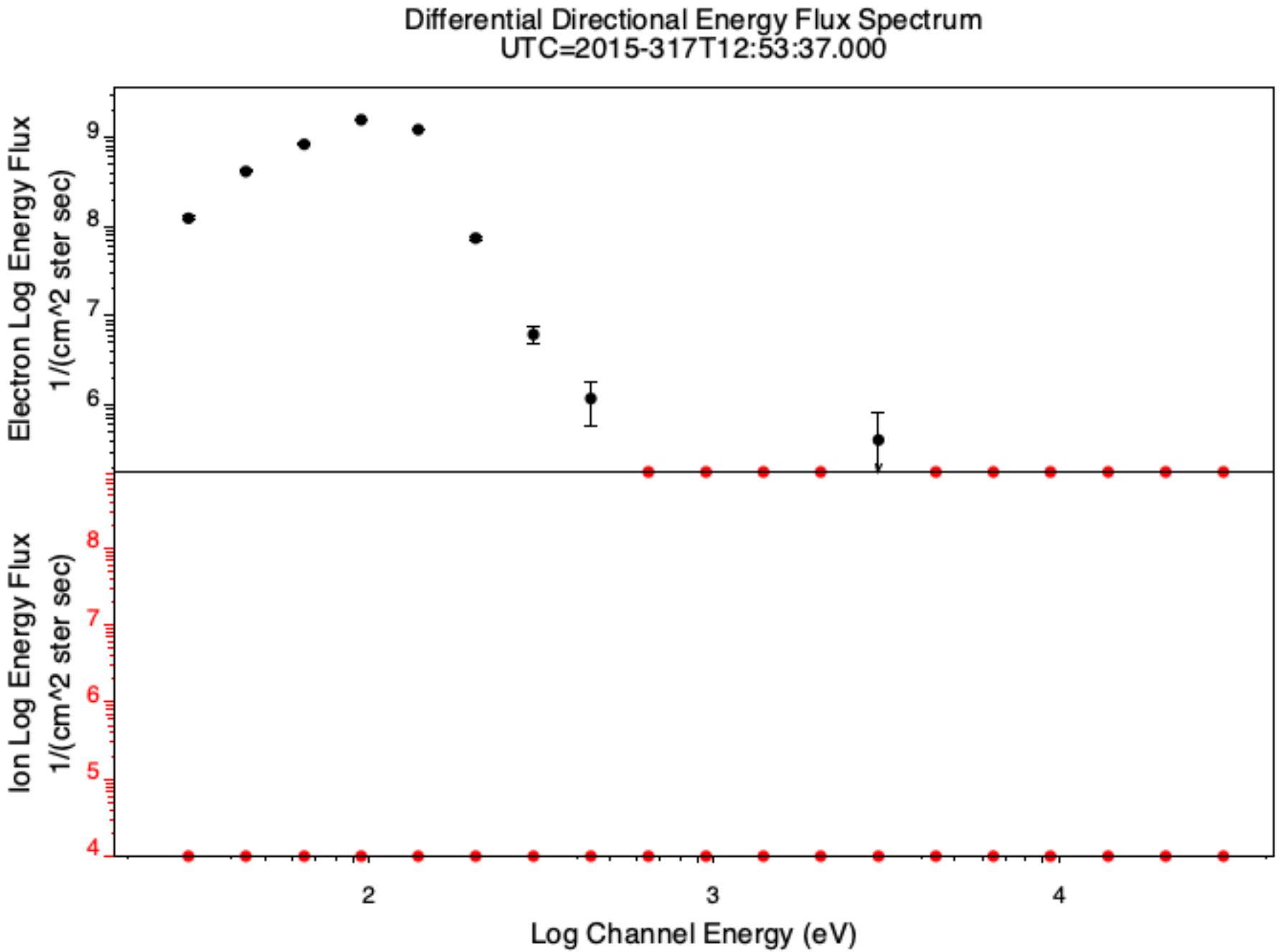

LAT: -81.32
LON: 184.03

MLAT: -77.89
MLT: 06:14

Electron JE: 1.62e+11
Avg E: 9.74e+01

Ion JE: 0.00e+00
Avg E: 0.00e+00

DMSP3.

F18

2015/317
Nov 13

Electrons
Log JE [eV/cm² s sr]

Avg E [eV]

Ions

Log Energy Flux [eV / (eV cm² s sr)]

Electrons

Log Energy [eV]

Ions

electrons ions

UT	12:45:00	12:48	12:51	12:54	12:57	13:00	13:03:00
LAT	-59.0	-68.9	-77.7	-81.2	-75.0	-65.6	-55.6
LON	264.5	255.2	233.3	175.2	130.8	115.1	107.6
MLAT	-50.0	-59.5	-69.3	-79.2	-88.3	-80.8	-70.7
MLT	06:40	06:36	06:28	06:10	02:31	20:13	19:51

JHU/APL

MIX South.

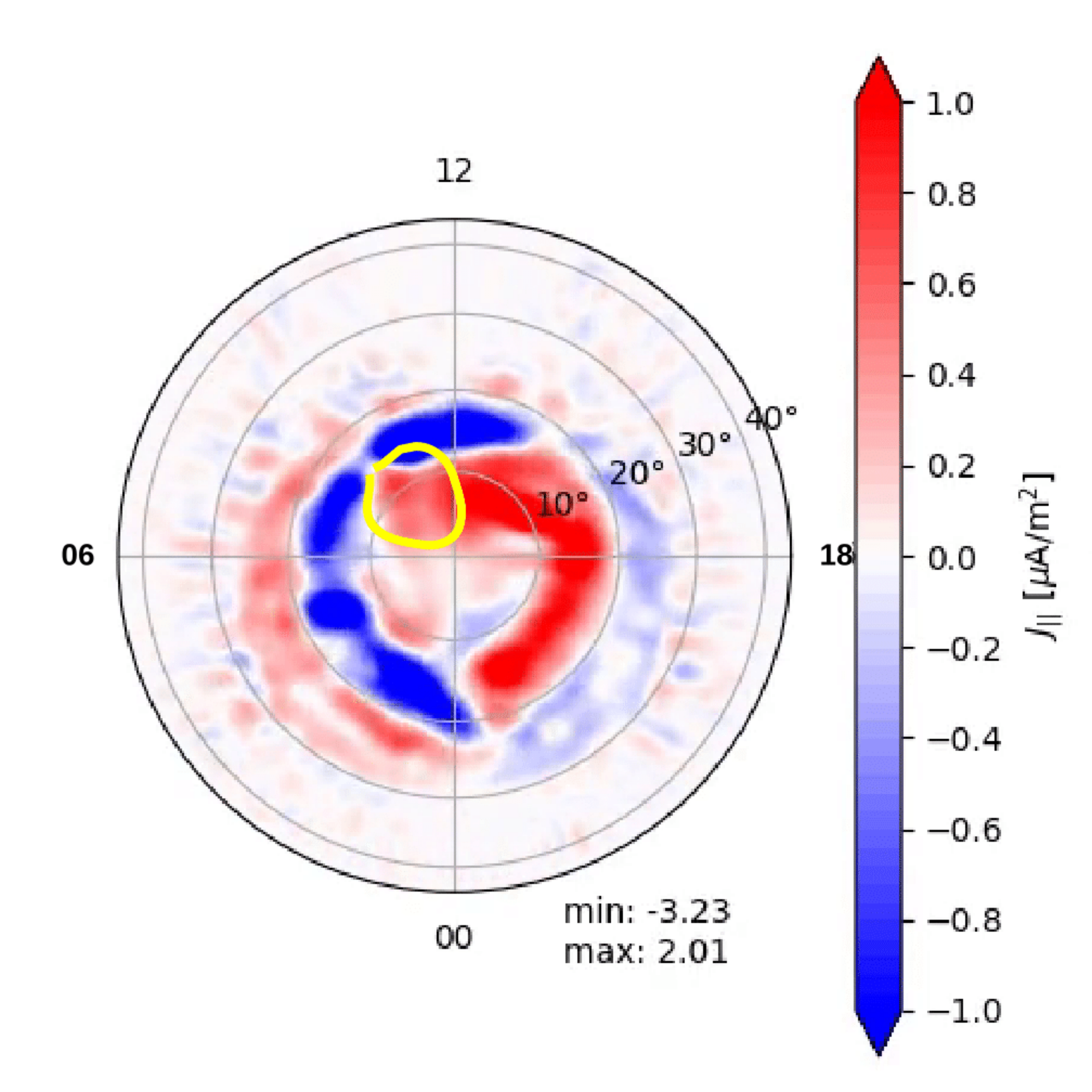
12
06
18
00
10°
20°
30°
40°
min: -3.23
max: 2.01
1.0
0.8
0.6
0.4
0.2
0.0
−0.2
−0.4
−0.6
−0.8
−1.0
$j_{\parallel}$ [μA/m^2]